Gd_5Si_4-PVDF nanocomposite films and their potential for triboelectric energy harvesting applications

S. M. Harstad[1] P. Zhao[2], N. Soin[2], A. A. El-Gendy[1,3], S. Gupta,[4] V. K. Pecharsky[4,5], J. Luo[2] and R. L. Hadimani[1, 6, 7*]

[1] Dept. of Mechanical and Nuclear Engineering, Virginia Commonwealth University, Richmond, VA, USA, 23284
[2] Institute for Materials Research and Innovation, University of Bolton, Bolton, UK, BL35AB
[3] Dept. of Physics, University of Texas El Paso, El Paso, TX, USA, 79968
[4] Div. of Materials Science and Engineering, Ames Laboratory, US Dept. of Energy, Ames, IA, USA, 50011
[5] Dept. of Materials Science and Engineering, Iowa State University, Ames, IA, USA, 50011
[6] Dept. of Biomedical Engineering Virginia Commonwealth University, Richmond, VA, USA, 23284
[7] Dept. of Electrical and Computer Engineering, Iowa State University, Ames, IA, USA, 50011

* rhadimani@vcu.edu

Abstract:
The triboelectric energy generators prepared using the combination of self-polarized, high β-phase nanocomposite films of Gd_5Si_4-PVDF and polyamide-6 (PA-6) films have generated significantly higher voltage of ~425 V, short-circuit current density of ~30 mA/m^2 and a charge density of ~116.7 μC/m^2 as compared to corresponding values of ~300 V, 30 mA/m^2 and 94.7 μC/m^2, respectively for the pristine PVDF-(PA-6) combination. The magnetic measurements of the Gd_5Si_4-PVDF films display a ferromagnetic behavior as compared to diamagnetic nature of pristine PVDF. The presence of magnetic nanoparticles in the polymeric matrix allows for some control over the microstructural properties during the preparation process. The results open new routes for multiferroic composite films to be suitable for multi-functional magnetic and triboelectric energy harvesting applications.

Introduction:
Recently, triboelectric generators (TEGs) have garnered much attention due to their high power output and conversion efficiency at a low production cost.[1-3] TEGs operate by accumulating static charge on the surfaces of different dielectric materials when they are brought into frictional contact with each other, which is then passed onto the external load *via* electrostatic induction using back electrodes.[1-5] In order to improve the energy density of TEGs, the dielectric materials should be diametrically opposite in their ability to provide or receive electrons in the triboelectric exchange i.e., one of the materials should lose electrons easily while the other readily accepts electrons.[1-3] Considering the triboelectric series, it can be observed that a triboelectric positive material such as polyamide-6 (PA6, Nylon) loses electrons when it is in contact with triboelectric negative polymer such as poly(vinylidene fluoride), PVDF, which has a significant ability to gain electrons due to the high electronegativity of the fluorine groups.[2], [3], [6], [7] As such, dielectric-dielectric TEGs based on the combination of fluorinated polymers and polyamides have been shown extensively.[6–8]

In this work, a TEG was prepared using the combination of tribo-negative Gd_5Si_4-PVDF and tribo-positive PA-6 films using a facile phase-inversion method. The fabricated Gd_5Si_4-PVDF TEGs showed significantly higher voltage of ~425 V, short-circuit current density of ~30 mA/m^2 and a charge density of ~116.7 μC/m^2 as compared to corresponding values of ~300 V, 30 mA/m^2 and 94.7 μC/m^2, respectively for the pristine PVDF-(PA-6) combination. The increase in the electrical output for the Gd_5Si_4-PVDF/PA-6 TEG system is attributed to the enhanced polarisation and β-phase content of the Gd_5Si_4-PVDF films. The work thus introduces a simple route for enhancing the polarisation and power output of TEGs without relying on prior charge injection technique and thus has the potential to be utilised further to making self-powered systems.

Preparation of Gd_5Si_4-PVDF composite films and assembling of TEG devices:

The synthesis of Gd_5Si_4 nanoparticles has been mentioned in detail elsewhere.[10]. The Gd_5Si_4-PVDF films were fabricated using a facile phase-inversion process. Further details of the process can be found in our earlier works [6], [11], [12][13]. During the quenching process, the Si substrate rested on a N50 neodymium iron boron permanent magnet, which provided a magnetic field that aligned the nanoparticles. The triboelectric counter surface films of polyamide-6 were synthesized using a 20 wt% dope solution of PA-6 in formic acid prepared *via* heating to 70 ºC under vigorous magnetic stirring. The spin coating and phase inversion parameters for PA-6 membranes can be found in our earlier works. [6, 10]

The 2 cm x 2 cm vertical contact mode TEG was assembled on an acrylic base wherein the first layer of PA-[6 film is attached using a conductive adhesive aluminium tape electrode. For the opposite side, either pristine PVDF or Gd_5Si_4-PVDF composite films were attached using conductive aluminium tape. These two substrates were then connected using two arc-shaped polyimide supports acting as spacers to maintain the desired spacing between them as shown in Fig. 1.

Characterization:

The as-prepared Gd_5Si_4 nanoparticle powders and the composite Gd_5Si_4-PVDF nanocomposite films were analyzed for their morphology using scanning electron microscopy and reported elsewhere [14]. The vibrational characteristics of the PVDF, Gd_5Si_4-PVDF and PA-6 films were examined by FTIR spectroscopy (Thermo Scientific IS10 Nicolet) wherein the spectra were recorded at a nominal resolution of ±1 cm^{-1} for a total of 64 scans. The calculation of β-phase content was carried out using vendor provided OMINIC software. Further characterization of the phase-inversion films was carried out using differential scanning calorimetry (DSC), to investigate the crystalline phase content using a TA Instruments DSC Q2000. The samples, approximate weight 2 mg, were heated at 10 ºC/min from 20 ºC to 200 ºC under 50 ml/min N_2 flow to assess their melting and crystalline behavior. The magnetic properties of the films were investigated using vibrating sample magnetometry in a Quantum Design Versalab. The electrical measurements of the TEG devices were carried out using a dynamic fatigue tester (Powil model YPS-1) in conjunction with a Tektronix MDO3022 oscilloscope and a Keysight B2981A picoammeter. The fatigue tester operates at various adjustable frequencies and loads between 1-1000N and allows for precise control over the impact load and frequencies.

Results and Discussion:

The presence of Gd_5Si_4 in the composite membranes was confirmed using X-ray photoelectron spectroscopy in the wide energy survey as well as core level scans (Fig. 2(a, b)). The core level Gd4d and Si2p spectra for the Gd_5Si_4-PVDF films confirmed the presence of magnetic Gd_5Si_4 particles in the matrix
The DSC thermograms for the pristine PVDF and Gd_5Si_4 composite films shown in Fig 2(c) provides evidence of the increase in the crystalline β-phase upon the addition of Gd_5Si_4 nanoparticles. The melting temperature, T_M, for the starting PVDF pellets and pristine PVDF membranes is in the range of 172-173 ^oC, with a slightly lower value for PVDF membranes. Upon the addition of Gd_5Si_4 nanoparticles to PVDF matrix, the T_M of the composite films shows a significant reduction to ~170 ^{o} C, with shoulder-like structures appearing at both low and high temperature regions. While there is ongoing debate on the exact melting temperatures of the various crystalline phases of PVDF, it is largely accepted that the β-phase melting occurs in the range 165–172 ^oC; α-phase crystals in the range 172–175^o C with the γ-phase melting between 175 and 180 ^oC (marked in Fig. 3(a)). [10-12] Considering the thermograms shown in Fig 2(c), it can be observed that for the composite Gd_5Si_4-PVDF membranes, they are largely enclosed within the range of the 165-170^o C, corresponding to the dominant β-phase. In fact, the T_M of the Gd_5Si_4-PVDF films is nearly 166.8^o C, which is approximately 3.0-5.0^o C lower as compared to that of pristine PVDF membranes and pellets, thus confirming that the lowering of the T_M can be attributed to the enhanced β-phase content of the films.The addition of Gd_5Si_4 nanoparticles to the PVDF matrix clearly leads to an increase in the crystallinity wherein the ΔX_C increased from ~38.6% for the PVDF pellets to approx. 46.8% (for pristine PVDF films) to nearly 62.0% for the 5wt% Gd_5Si_4-PVDF films calculated from the literature [10-12]. Since both the pristine and Gd_5Si_4 membranes were prepared using the phase inversion process, while the slow liquid-liquid de-mixing of DMF and deionised water provides longer crystallisation times, the nucleation effects provided by the Gd_5Si_4 nanoparticles are believed to be responsible for the significant enhancement of the crystalline phase. [10, 12, 13]
The FTIR spectra of the PVDF pellets, pristine PVDF and Gd_5Si_4-PVDF composite membranes is shown in Fig. 2(d) wherein the quantification of the piezoelectric β-phase relative to the α-phase was carried out using the signature vibrational bands at 840 cm^{-1} (CH_2 rocking Magnetic field (kOe) and CF_2 asymmetric stretching vibration) and 760 cm^{-1} (CF_2 bending and skeletal bending), respectively [6, 10-12]. It can be observed that upon phase inversion, a significant increase in the β-phase is observed for the PVDF membranes, wherein the β-phase is enhanced to ~49% from an initial value of ~39% for the starting PVDF pellets. With the introduction of Gd_5Si_4 nanoparticles, under the same processing conditions, the β-phase is further enhanced to ~79%. The values obtained in this work are very similar to our earlier reported works.[14]
Fig. 3 shows the measurement of magnetization vs. temperature in the range of 200-380 K and at an applied field of 100 Oe. While the pristine PVDF films show a diamagnetic behavior; the nanocomposite Gd_5Si_4-PVDF films were ferromagnetic below 310K and showed a transition around this temperature. Inset of Fig. 3 shows the hysteresis measurement at room temperature wherein it can be clearly seen that the films are ferromagnetic at room temperature with negligible coercivity. The ferromagnetic behavior of the film is attributed the presence of Gd_5Si_4 nanoparticles in the composite film wherein the diamagnetic behavior of the pristine PVDF film is overcome by the large magnetic moment of ferromagnetic Gd_5Si_4 nanoparticles.

TEG electrical testing:

The TEGs fabricated with the Gd_5Si_4 nanocomposite films and pristine PVDF (as reference) was tested for their triboelectric output using a dynamic fatigue tester. The intrinsic output characteristics of open-circuit voltage (V_{oc}) and short circuit current density (J_{sc}), of TEGs were measured to represent the electrical output of the TEGs. Voltage measurements were taken at impact forces ranging from 20-80 N at a constant frequency of 5 Hz and a spacer distance of 8 cm. As illustrated in Fig.4 (a & b), the voltage response of both Gd_5Si_4-PVDF and pristine PVDF TEGs increases almost linearly with the applied force. Moreover, it was observed that the average peak-to-peak V_{oc} of the Gd_5Si_4-PVDF TEG (~200 V) at 20 N impact force condition is around 1.3 times greater than the peak-to-peak V_{oc} of pristine PVDF (~150 V) tested at the same conditions. With the increase in the force, the variation of the outputs from the two devices increased to ~1.5 times across the range, with maximum Voc values of 425 V and 350 V for Gd_5Si_4-PVDF TEG and pristine PVDF TEG, respectively.

From the above equation, it can be clearly observed that the V_{oc} is directly proportional to the spacer distance and the surface charge density (see Fig. 4(b) inset for the variation of the output V_{oc} at two different spacer values). This variation in the V_{oc} can also be explained considering the mechanical and elastic properties of the porous PA6 and Gd_5Si_4-PVDF membranes, wherein an increase in the impact force causes a larger interfacial deformation and filling of the vacant pores, leading to a larger effective contact charging area and therefore higher surface charge density and thus higher open circuit voltage. [6].

Considering the short circuit current density curves shown in Fig.4, at low impact conditions (20-60 N), the observed current density from the Gd_5Si_4-PVDF TEG was ~5 mA/m^2 lower than the values observed from the pristine PVDF TEG. However, with the increase in the impact force to 80N, a rapid increase in the J_{sc} was observed wherein the current density values reached almost the same level as that of the pristine TEGs. The calculated charge densities were consistently observed to be higher for the Gd_5Si_4-PVDF films than as compared to the pristine PVDF TEGs. Typically, at lower force values (20, 40N), the calculated charge densities for the pristine and Gd_5Si_4-PVDF TEG systems were ~37.5 and 60.0 $\mu C/m^2$, respectively which upon increase in the force to 80N were enhanced to 94.7 and 116.7 $\mu C/m^2$, respectively. This increase in the charge density can be attributed the nucleation effects provided by the Gd_5Si_4 nanoparticles leading to the enhanced β-phase and crystallinity.

Fig. 5 shows the voltage response of the Gd_5Si_4-PVDF TEG as functions of impact frequency (1-9 Hz) at the fixed working conditions of ~40 N impact force and 4 cm spacer distance. It is obvious that the electrical output values of the Gd_5Si_4-PVDF are almost proportional to the growth of the working frequency at low working frequency condition (1 to 5 Hz), wherein the V_{oc} increased from approximately 25 V to 175 V with the corresponding increase in J_{SC} from approximately 0.9 mA/m^2 to 18 mA/m^2. As the working frequency was increased from 5 Hz to 9 Hz, no significant increase in output voltage could be observed; correspondingly, the increase in the current density across this range also slowed down sharply, which could be due to the insufficient contact and transmission of force at higher frequencies. To confirm the mechanical stability of TEG fabricated by Gd_5Si_4-PVDF film, a stability test was performance by operating the TEG at the working condition of 5 Hz frequency, 4 cm spacer distance and 80 N impact force for 10,000 cycles. By observing the test results shown in Fig. 5(c), the TEG device displayed a stable power generation performance for long-duration operation. The output voltage was maintained around 400 V without any visible attenuation. It should be mentioned that the peak values of V_{oc} measured in the period around 4000 cycles arbitrarily increased to approximately 450 V and slowly decreased to approximately 400 V within 4,000 operation cycles. Thus, the enhanced output from the

Gd_5Si_4-PVDF based TEG device is largely stable, making it useful for applications in energy harvesting from low-medium frequency impact applications.

Conclusions:

Triboelectric nanogenerators were fabricated from aligned Gd_5Si_4-PVDF nanocomposites. Gd_5Si_4-PVDF films were synthesized by phase-inversion technique in the presence of an external magnetic field that aligned the magnetic Gd_5Si_4 nanoparticles during spin-coating process. These aligned films Gd_5Si_4-PVDF showed significantly higher crystallinity and increased β-phase fraction as compared to the pristine PVDF films. The assembled TEGs using Gd_5Si_4-PVDF films against a PA-6 counter material was shown to provide Voc values of ~425V, short circuit current density of ~30 mA/m^2 and a charge density of ~116.7 μC/m^2 as compared to corresponding values of ~300 V, 30 mA/m^2 and 94.7 μC/m^2, respectively for the pristine PVDF-(PA-6) combination. The higher values of V_{oc} and more importantly the charge density show the beneficial effects of the addition of Gd_5Si_4 nanoparticles to the PVDF matrix in enhancing the polarization of the nanocomposites and providing routes for controlling the crystallization and formation of the piezoelectric β-phase in PVDF. Further development of these pathways can lead to highly efficient TEGs capable of harvesting electrical energy from low-frequency mechanical impacts.

Acknowledgements:

Synthesis and materials processing at the Ames Laboratory was supported by the Office of Basics Energy Sciences, Materials Science and Engineering Division of the U.S. Department of Energy (DOE). The Ames Laboratory is operated for the U.S. DOE by Iowa State University of Science and Technology under contract No. DE-AC02-07CH11358. Work at VCU was partially funded by National Science Foundation, Award Numbers: 1357565, 1610967 and 1726617.

References:

[1] Z. L. Wang, J. Chen, and L. Lin, "Progress in triboelectric nanogenerators as a new energy technology and self-powered sensors," *Energy Environ. Sci.*, vol. 8, no. 8, pp. 2250–2282, 2015.

[2] S. Wang, L. Lin, and Z. L. Wang, "Triboelectric nanogenerators as self-powered active sensors," *Nano Energy*, vol. 11, pp. 436–462, 2015.

[3] Z. L. Wang, "Self-powered nanosensors and nanosystems," *Adv. Mater.*, vol. 24, no. 2, pp. 280–285, 2012.

[4] F. R. Fan, Z. Q. Tian, and Z. Lin Wang, "Flexible triboelectric generator," *Nano Energy*, vol. 1, no. 2, pp. 328–334, 2012.

[5] S. Niu, X. Wang, F. Yi, Y. S. Zhou, and Z. L. Wang, "A universal self-charging system driven by random biomechanical energy for sustainable operation of mobile electronics.," *Nat Commun*, vol. 6, p. 8975, 2015.

[6] N. Soin, P. Zhao, K. Prashanthi, J. Chen, P. Ding, E. Zhou, T. Shah, S. C. Ray, C. Tsonos, T. Thundat, E. Siores, and J. Luo, "High performance triboelectric nanogenerators based on phase-inversion piezoelectric membranes of poly(vinylidene fluoride)-zinc stannate (PVDF-ZnSnO3) and polyamide-6 (PA6)," *Nano Energy*, vol. 30, pp. 470–480, 2016.

[7] R. L. Hadimani and E. Siores, "Piezoelectric Polymer Element and Production Method and Apparatus," PCT/GB2011/051734, 23-Mar-2012.

[8] Z. Wang, L. Cheng, Y. Zheng, Y. Qin, and Z. L. Wang, "Enhancing the performance of triboelectric nanogenerator through prior-charge injection and its application on self-powered anticorrosion," *Nano Energy*, vol. 10, pp. 37–43, 2014.

[9] Z. Li, J. Shen, I. Abdalla, J. Yu, and B. Ding, "Nanofibrous membrane constructed wearable triboelectric nanogenerator for high performance biomechanical energy harvesting," *Nano Energy*, vol. 36, no. April, pp. 341–348, 2017.

[10] R. L. Hadimani, S. Gupta, S. M. Harstad, V. K. Pecharsky, and D. C. Jiles, "Investigation of Room Temperature Ferromagnetic Nanoparticles of Gd5Si4," *IEEE Trans. Magn.*, vol. 51, no. 11, pp. 5–8, 2015.
[11] C. Tsonos, N. Soin, G. Tomara, B. Yang, G. C. Psarras, A. Kanapitsas, and E. Siores, "Electromagnetic wave absorption properties of ternary poly(vinylidene fluoride)/magnetite nanocomposites with carbon nanotubes and graphene," *RSC Adv.*, vol. 6, no. 3, pp. 1919–1924, 2016.
[12] C. Tsonos, C. Pandis, N. Soin, D. Sakellari, E. Myrovali, S. Kripotou, A. Kanapitsas, and E. Siores, "Multifunctional nanocomposites of poly(vinylidene fluoride) reinforced by carbon nanotubes and magnetite nanoparticles," *Express Polym. Lett.*, vol. 9, no. 12, pp. 1104–1118, 2015.
[13] N. Soin, D. Boyer, K. Prashanthi, S. Sharma, a. a. Narasimulu, J. Luo, T. H. Shah, E. Siores, and T. Thundat, "Exclusive self-aligned β-phase PVDF films with abnormal piezoelectric coefficient prepared via phase inversion," *Chem. Commun.*, vol. 2, pp. 1–4, 2015.
[14] S. M. Harstad, N. D'Souza, N. Soin, A. A. El-Gendy, S. Gupta, V. K. Pecharsky, T. Shah, E. Siores, and R. L. Hadimani, "Enhancement of beta phase in PVDF films embedded with ferromagnetic Gd5Si4 nanoparticles for piezoelectric energy harvesting," *AIP Adv.*, vol. 7, p. 056411, 2017.

Fig. 1 Triboelectric Generator Configuration based on PA-6 membrane and nanocomposite PVDF membrane.

Fig. 2 (a-f): (a) Wide energy survey spectra (WESS) XPS spectra with the inset showing the Si 2p core level spectra for 5 wt% Gd_5Si_4-PVDF films, (b) C1s core level spectra with the inset showing the Gd4d core level spectra for the 5 wt% Gd_5Si_4-PVDF films, (c) DSC thermograms with the melting zones of α, β and γ phases marked out, (d) FTIR spectroscopy measurements showing the enhancement of the β-phase with the addition of Gd_5Si_4 and (e and f) transmission spectra showing the shifts in the CH_2 symmetric and asymmetric mode of pristine PVDF and 5 wt% Gd_5Si_4-PVDF films.

Fig. 3 Magnetization vs. Temperature at an applied field of 100Oe of Gd_5Si_4-PVDF films. Inset Magnetization vs. magnetic field at room temperature. Note, the hysteresis graph doesn't show observable coercivity.

Fig. 4. TEG electrical characteristics of open-circuit voltage values for (a) pristine PVDF TEG and (b) Gd_5Si_4-PVDF TEG; short circuit current density of (c) pristine PVDF-TEG and (d) Gd_5Si_4-PVDF TEG. The inset of (b) shows the variation of the V_{oc} as a function of spacer distance for a 40 N impact force.

Fig. 5. The electrical output of Gd_5Si_4-PVDF TEG at a fixed impact force of 40 N and spacer distance of 4 cm with the working frequency range from 1Hz to 9Hz, (a) open-circuit voltage, (b) short-circuit current density with and (c) operational stability of Gd_5Si_4-PVDF TEG operated continuously for 10,000 cycles, acquired at 80 N, 8 cm spacing and 5 Hz working frequency.

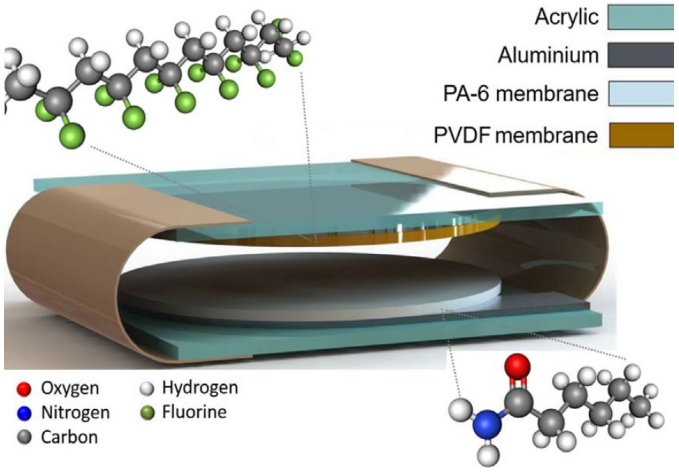

Fig. 1 Triboelectric Generator Configuration based on PA-6 membrane and nanocomposite PVDF membrane.

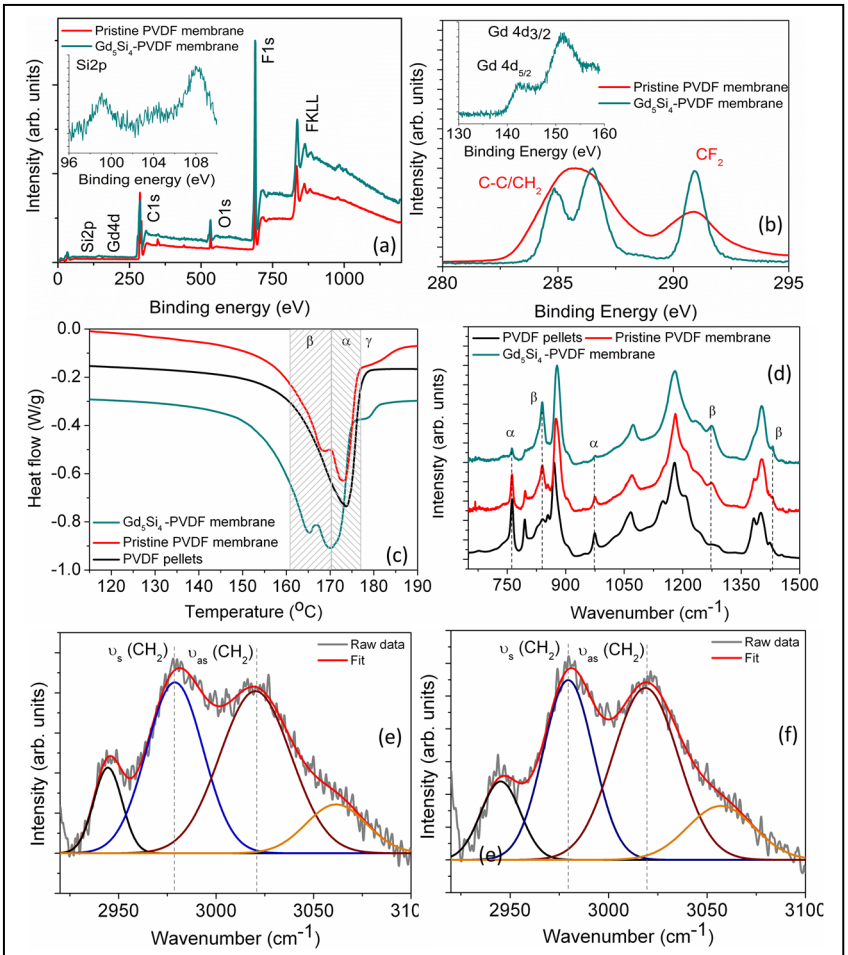

Fig. 2 (a-f): (a) Wide energy survey spectra (WESS) XPS spectra with the inset showing the Si 2p core level spectra for 5 wt% Gd_5Si_4-PVDF films, (b) C1s core level spectra with the inset showing the Gd4d core level spectra for the 5 wt% Gd_5Si_4-PVDF films, (c) DSC thermograms with the melting zones of α, β and γ phases marked out, (d) FTIR spectroscopy measurements showing the enhancement of the β-phase with the addition of Gd_5Si_4 and (e and f) transmission spectra showing the shifts in the CH_2 symmetric and asymmetric mode of pristine PVDF and 5 wt% Gd_5Si_4-PVDF

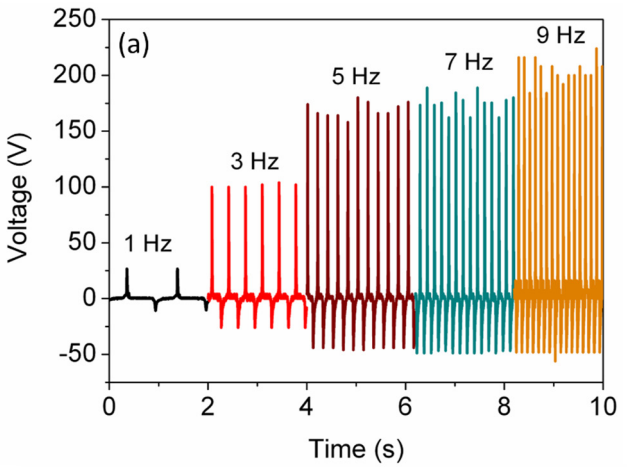

Fig. 3 Magnetization vs. Temperature at an applied field of 100Oe of Gd_5Si_4-PVDF films. Inset Magnetization vs. magnetic field at room temperature. Note, the hysteresis graph doesn't show observable

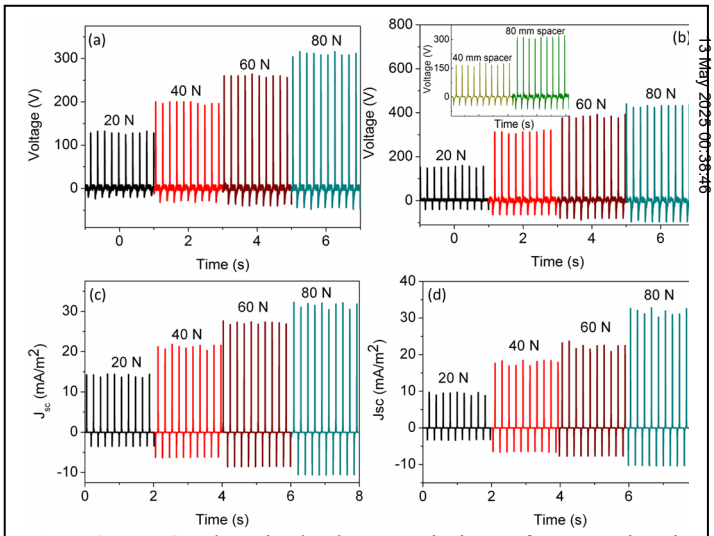

Fig. 4. TEG electrical characteristics of open-circuit voltage values for (a) pristine PVDF TEG and (b) Gd_5Si_4-PVDF TEG; short circuit current density of (c) pristine PVDF-TEG and (d) Gd_5Si_4-PVDF TEG. The inset of (b) shows the variation of the V_{oc} as a function of spacer distance for a 40 N impact force.

Fig. 5. The electrical output of Gd_5Si_4-PVDF TEG at a fixed impact force of 40 N and spacer distance of 4 cm with the working frequency range from 1Hz to 9Hz, (a) open-circuit voltage, (b) short-circuit current density with and (c) operational stability of Gd_5Si_4-PVDF TEG operated continuously for 10,000 cycles, acquired at 80 N, 8 cm spacing and 5 Hz working